Chinese Chemical Letters 37 (2026) 111155

Contents lists available at ScienceDirect

Chinese Chemical Letters

journal homepage: www.elsevier.com/locate/cclet

Assessing the photoluminescence of metal nanoclusters: The individual *versus* the collective

Xiaoqin Du, Peiyao Pan, Haoqi Li, Di Zhang, Wentao Huang, Xi Kang*, Manzhou Zhu

Department of Chemistry and Centre for Atomic Engineering of Advanced Materials, Key Laboratory of Structure and Functional Regulation of Hybrid Materials of Ministry of Education, Anhui Province Key Laboratory of Chemistry for Inorganic/Organic Hybrid Functionalized Materials, Anhui University, Hefei 230601, China

ARTICLE INFO

Article history:
Received 23 February 2025
Revised 20 March 2025
Accepted 27 March 2025
Available online 27 March 2025

Keywords:
Nanocluster
Photoluminescence
Crystal structure
Ligand effect
Intermolecular interaction

ABSTRACT

Understanding the photoluminescence (PL) mechanism of metal nanoclusters from both molecular and supramolecular perspectives is crucial for developing highly emissive cluster-based nanomaterials. In this study, we synthesized two structurally similar Ag_{14} nanoclusters with different phosphine stabilizers, which demonstrated opposite PL behaviors in solution and crystalline states. The Ag_{14} nanocluster stabilized by $P(Ph\text{-}OMe)_3$ ligands exhibited a higher PL intensity compared to the one stabilized by $P(Ph\text{-}F)_3$ ligands, which was attributed to the stronger electron-donating ability of the $P(Ph\text{-}OMe)_3$ ligand that improved ligand-to-metal charge transfer efficiency. In contrast, the $P(Ph\text{-}F)_3$ stabilized Ag_{14} crystals displayed greater PL intensity than the Ag_{14} cluster crystal with a -OMe surface, which was due to stronger intermolecular interactions within the cluster lattice of the former that limited non-radiative energy loss and thus enhanced PL. Overall, this work aims to promote a comprehensive understanding of the fluorescence in cluster-based nanomaterials, which will be beneficial for their downstream applications.

© 2025 Published by Elsevier B.V. on behalf of Chinese Chemical Society and Institute of Materia Medica, Chinese Academy of Medical Sciences.

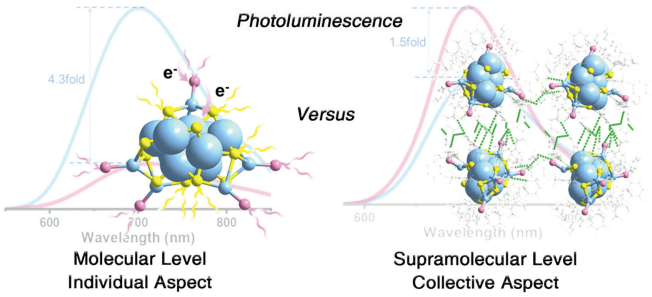
Metal nanoclusters, also known as ultra-small metal nanoparticles, represent an emerging class of atomically precise nanomaterials that bridge the gap between discrete atoms and plasmonic nanomaterials [1–7]. Due to their quantum size effects and unique electronic states, nanoclusters exhibit fascinating physical and chemical properties, such as photoluminescence (PL), chirality, magnetism, catalysis, and electrochemistry [8–28]. Among these properties, PL stands out as one of the most intriguing characteristics of metal nanoclusters. The well-defined composition and atomically precise structures of these clusters are essential for understanding the relationship between structure and photoluminescence. This understanding is also critical for the rational design of cluster-based nanomaterials that can achieve enhanced PL quantum yields (QY) and tunable emission wavelengths, setting them apart from conventional PL materials.

So far, various emissive nanoclusters have been synthesized, and several effective strategies have been developed to control their PL properties [29–34]. These strategies include alloying, ligand engineering, aggregation-induced emission (AIE), and the construction of cluster-based networks. Among these methods, ligand engineering has emerged as a particularly effective approach for enhancing PL QY and adjusting the emission wavelengths of nanoclusters. The electronic and steric properties of the peripheral ligands significantly influence the electronic and geometric structures of the nanoclusters, as well as their optical performance. It is also important to note that the discussions thus far primarily focus on the PL behavior of nanoclusters in their solution states, emphasizing their individual molecular characteristics [35–38].

Indeed, most emissive nanoclusters exhibit complex PL behavior in various states, which requires analyzing their PL from a supramolecular perspective, especially when in crystalline states. Typically, the energy dissipation of excited nanoclusters occurs through two main pathways: (1) Radiative transitions, primarily *via* PL, and (2) non-radiative transitions, which are influenced by intramolecular or intermolecular vibrations. It is generally accepted that ordered aggregation reduces energy loss from excited clusters through non-radiative transitions, thereby enhancing energy dissipation through radiative transitions, *i.e.*, *via* PL. Previous studies have indicated that the enhanced intermolecular and intramolecular interactions, regulated by the arrangement of ligands, are the primary reasons for the PL enhancement of metal nanoclusters in their aggregated states, with the restriction of intermolecular motion playing a crucial role. In this context, the factors influencing the PL of metal nanoclusters can be understood through two aspects: the electronic and geometric structures are related to the molecular chemistry of nanocluster solutions, while supramolecu-

* Corresponding author.
E-mail address: kangxi_chem@ahu.edu.cn (X. Kang).

https://doi.org/10.1016/j.cclet.2025.111155
1001-8417/© 2025 Published by Elsevier B.V. on behalf of Chinese Chemical Society and Institute of Materia Medica, Chinese Academy of Medical Sciences.



Scheme 1. Assessing the photoluminescence of metal nanoclusters from both the individual (molecular) and collective (supramolecular) aspects.

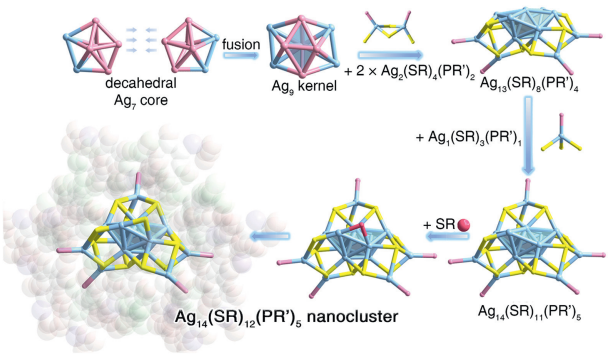


Fig. 1. Structural anatomy of Ag_{14}-OMe and Ag_{14}-F nanoclusters. Color labels: blue/pink = Ag; yellow/red = S; Pale pink = P. All C and H atoms were omitted for clarity.

lar chemistry primarily pertains to their aggregated states. These two aspects are complementary and should be considered together to fully understand the PL behavior of metal nanoclusters [39–44].

In this study, we prepared two structurally comparable Ag_{14} nanoclusters that have the same metallic core but different phosphine peripheral ligands: $Ag_{14}[SPh(CF_3)_2]_{12}[P(Ph\text{-}OMe)_3]_5$ (referred to as Ag_{14}-OMe) and $Ag_{14}[SPh(CF_3)_2]_{12}[P(Ph\text{-}F)_3]_5$ (referred to as Ag_{14}-F). We assessed the PL of these two nanoclusters in both their solution and crystalline states, examining how different structural factors influence their emission properties (Scheme 1). In the solution state, Ag_{14}-OMe exhibited a higher PL intensity than Ag_{14}-F. This difference was attributed to the stronger electron-donating ability of the $P(Ph\text{-}OMe)_3$ ligand compared to $P(Ph\text{-}F)_3$, which affected the ligand-to-metal charge transfer efficiency. However, when comparing the crystalline states, Ag_{14}-F displayed a stronger PL intensity than Ag_{14}-OMe. This enhancement was due to greater intermolecular interactions within the Ag_{14}-F lattice, which restricted non-radiative energy loss and thus boosted PL. These findings provide important insights into the fluorescence behavior of metal nanoclusters at both the molecular and supramolecular levels.

The Ag_{14}-OMe nanocluster was synthesized by directly reducing the Ag-$SPh(CF_3)_2$-$P(Ph\text{-}OMe)_3$ complexes with $NaBH_4$ (see Supporting information for more details). The synthesis of the Ag_{14}-F nanocluster was the same as that of Ag_{14}-OMe except that $P(Ph\text{-}OMe)_3$ was replaced by $P(Ph\text{-}F)_3$. Single crystals of the two nanoclusters were cultivated at room temperature by liquid diffusing the *n*-hexane into a CH_2Cl_2 solution containing each nanocluster. After 14 days, red crystals were collected, and the structures of the two nanoclusters were determined by single-crystal X-ray diffraction (SC-XRD). The Ag_{14}-OMe nanocluster was crystallized in a triclinic crystal system with a *P*-1 space group, whereas Ag_{14}-F nanocluster was crystallized in a monoclinic crystal system with a *I*2/a space group (Tables S1 and S2 in Supporting information). The compositions of Ag_{14}-OMe and Ag_{14}-F nanoclusters were further confirmed by X-ray photoelectron spectroscopy measurements (Fig. S1 in Supporting information).

Structurally, the Ag_{14}-OMe and Ag_{14}-F nanoclusters exhibited the same overall framework but different peripheral phosphine ligands. Specifically, the Ag_{14} nanocluster featured an Ag_9 kernel, which could be viewed as two Ag_7 decahedra fused by sharing a common Ag_4 face. The Ag_9 kernel was stabilized by two $Ag_2(SR)_4(PR')_2$ motif-like units through Ag-S and Ag-Ag interactions, forming an $Ag_{13}(SR)_4(PR'_3)_4$ structure ($SR = SPh(CF_3)_2$; $PR' = P(Ph\text{-}OMe)_3$ or $P(Ph\text{-}4\text{-}F)_3$). Furthermore, a single $Ag_1(SR)_3(PR')_1$ surface unit was anchored onto the top of the nanocluster framework, resulting in the $Ag_{14}(SR)_{11}(PR'_3)_5$ framework. Moreover, a bare thiol ligand connected the Ag_9 kernel *via* μ_2-S interactions, giving rise to the overall structure of the Ag_{14} nanocluster (Fig. 1).

Although the two Ag_{14} nanoclusters exhibited the same cluster framework, their different peripheral phosphine ligands led to comparable configurations in terms of the corresponding bond lengths. The average Ag-Ag bond length in the Ag_9 kernel of Ag_{14}-OMe was 2.965 Å, which decreased to 2.943 Å in Ag_{14}-F. In addition, the corresponding bond lengths of peripheral subunits were similar–the average bond lengths of Ag(kernel)-S(motif), Ag(motif)-P(motif), and Ag(motif)-S(motif) for the Ag_{14}-OMe nanocluster was determined as 2.559, 2.398, and 2.693 Å, respectively, and those of the Ag_{14}-F nanocluster was 2.559, 2.398, and 2.693 Å, respectively (Fig. S2 in Supporting information). In this context, the change of peripheral phosphine ligands slightly altered the geometric structure of Ag_{14} nanoclusters while maintaining their overall framework.

The Ag_{14}-OMe and Ag_{14}-F nanoclusters exhibited similar crystalline packing patterns. As shown in Figs. S3 and S4 (Supporting information), each crystal unit contained two nanocluster molecules that were assigned as enantiomeric isomers. In this context, the cluster crystals were racemic. The cluster enantiomers were organized into a lamellar eutectic in the (010), (100), and (001) planes *via* a layer-by-layer arrangement. Fig. S5 (Supporting information) showed the crystalline arrangement of the Ag_{14}-OMe nanocluster superlattices. Notably, the cluster molecules with the same chiral configurations were neatly and linearly assembled along all three directions, and the stacking sequence was the "ABAB". The average interlayer distance of the lamellar eutectic for Ag_{14}-OMe was determined as 18.207 Å. In comparison, although Ag_{14}-F showed the same "ABAB" crystalline packing as that of Ag_{14}-OMe, the average interlayer distance of the lamellar eutectic for Ag_{14}-F decreased to 17.724 Å (Fig. S6 in Supporting information), indicating its more compact intramolecular packing mode relative to that of Ag_{14}-OMe. Indeed, the abundant fluoride-triggered i1ntercluster interactions contributed to the more compact supramolecular packing of the Ag_{14}-F (discussed below), which in turn reduced the interlayer distance of its crystalline lattice.

Electrospray ionization mass spectrometry (ESI-MS) was performed to analyze the chemical composition of the nanoclusters. As illustrated in Fig. S7 (Supporting information), the mass result in the negative mode for the Ag_{14}-F nanocluster presented three peaks at 2519.31, 2677.35, and 2835.38 Da. The interval between the isotope peaks was $m/z = 0.5$, confirming the "-2"-charge state of the detected molecules. In this context, the three mass signals corresponded well to $[Ag_{14}(C_{18}H_{12}F_3P)_x((CF_3)_2C_6H_3S)_{11}(CH_2Cl_2)_1(CH_3OH)_1(CH_3CH_2OH)_1Cl_1]^{2-}$, where *x* ranged from 2-4. Due to the instability of Ag_{14}-OMe in the presence of methanol, the ESI-MS detection of this nanocluster was unsuccessful. However, the same configuration and composition

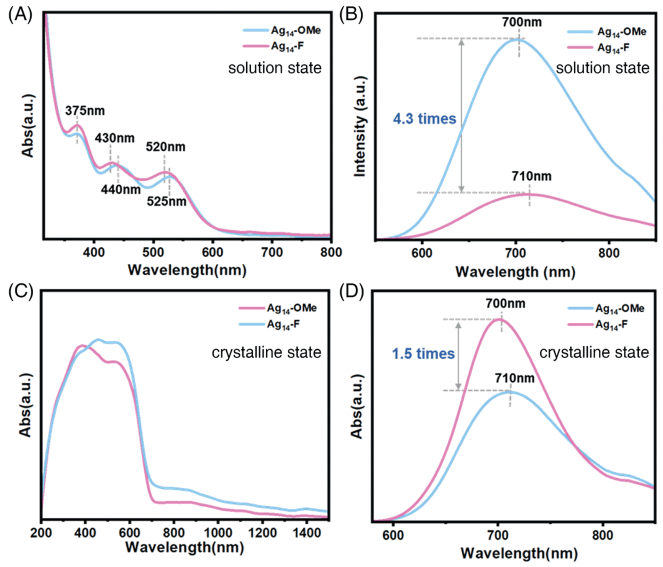


Fig. 2. Optical properties of Ag_{14}-OMe (blue lines) and Ag_{14}-F (pink lines) nanoclusters. (A) Comparison of optical absorption of Ag_{14}-OMeand Ag_{14}-F nanoclusters dissolved in CH_2Cl_2. (B) Comparison of PL properties of Ag_{14}-OMe and Ag_{14}-F nanoclusters dissolved in CH_2Cl_2. (C) Comparison of optical absorption of Ag_{14}-OMe and Ag_{14}-F nanocluster crystals. (D) Comparison of PL properties of Ag_{14}-OMe and Ag_{14}-F nanocluster crystals.

of the two nanoclusters suggested their identical numbers of free valence electrons as 4, *i.e.*, 14(Ag) – 11(SR) – 1(Cl) + 2(charge) = 4 electrons.

The same framework of the two Ag_{14} nanoclusters rendered them ideal platforms for assessing the structure-property correlations. The ultraviolet-visible (UV-vis) spectrum of Ag_{14}-OMe (dissolved in CH_2Cl_2) displayed continuous optical absorptions with three distinct peaks at 375, 440, and 525 nm. In comparison, Ag_{14}-F exhibited absorption peaks at 375, 430, and 520 nm. In this context, the optical absorptions of Ag_{14}-F showed a slight blue shift relative to those of Ag_{14}-OMe, which originated from their different peripheral phosphine ligands (Fig. 2A). In addition, the very analogous UV-vis spectrum profile of the two nanoclusters demonstrated their similar electronic structures. Besides, the optical absorptions of the two nanoclusters remained unchanged after 9 months in the air, demonstrating their high stability (Figs. S8A and B in Supporting information).

The two Ag_{14} nanoclusters fluoresced when illuminated at 375 nm. The PL excitation spectra of the nanoclusters resembled their absorption spectra (Fig. S8C in Supporting information), which further suggested their molecular nature and have been observed in several previously reported metal nanoclusters [45,46]. Through the modification of their peripheral phosphine ligands, the PL emission of Ag_{14}-OMe was observed at 700 nm in its CH_2Cl_2 solution, whereas the emission of Ag_{14}-F exhibited a red shift to 710 nm (Fig. 2B). Besides, the PL intensity of Ag_{14}-OMe was 4.3 times greater than that of Ag_{14}-F. First, since the 4.3-fold PL emissions were detected from their solution states, the origin of such a PL difference should be rationalized from the molecular level. Second, the homologous geometric/electronic structures and PL lifetimes (Figs. S9A and B in Supporting information) of the two Ag_{14} nanoclusters demonstrated their similar electronic transition from the lowest unoccupied molecular orbital (LUMO) to the highest occupied molecular orbital (HOMO), and the different PL emission was not from their HOMO-LUMO gap differences. In this context, the superior PL intensity of Ag_{14}-OMe in the solution state could be attributed to its peripheral $P(Ph\text{-}OMe)_3$ ligand. Compared to $P(Ph\text{-}F)_3$ ligands, $P(Ph\text{-}OMe)_3$ ligands, which contain -OMe terminal groups, demonstrated a greater ability to donate electrons. This strengthened electron-donating capability probably increased the electronic transitions between ligands and metals in the cluster framework and thus enhanced the emission intensity of Ag_{14}-OMe at the molecular level. Accordingly, the PL of the Ag_{14} nanocluster was caused by charge transfer between the aromatic groups on phosphine ligands and the metallic kernel of the nanocluster, *i.e.*, the ligand-to-metal charge transfer (LMCT), which was frequently determined as the PL mechanism of previously reported fluorescent nanoclusters [47,48]. In this context, the PL intensity of the Ag_{14} nanocluster in the solution state was manipulated by modulating the electron-donating ability of the peripheral phosphine ligands.

The photophysical properties of nanocluster crystals were further evaluated. The optical absorptions were similar for the two clusters in their crystalline state, further demonstrating their analogous electronic structures and crystalline packing modes (Fig. 2C). Besides, for the PL, the emission wavelength of Ag_{14}-OMe crystals showed a 10 nm red shift compared with its solution; however, a 10 nm blue shift was observed by comparing the emission wavelength of Ag_{14}-F crystals with its solution (Figs. 2B and D). In addition, the PL lifetimes of Ag_{14}-OMe and Ag_{14}-F crystals were 28.3 and 1.1 μs (Figs. S9C and D in Supporting information), respectively, both falling in the microsecond range, which were remarkably longer than the cluster solutions (5 and 1.5 ns, respectively). In this context, the nanocluster crystals exhibited apparent differences in optical absorptions, emission wavelengths, and PL lifetimes relative to their solutions. Such differences in photophysical properties of Ag_{14} nanoclusters in different forms, *i.e.*, solution and crystalline states, arose from distinct combinations of the electronic coupling and the lattice-origin, non-radiative decay pathways occurring through electron-phonon interactions [49–51].

Significantly, the PL intensity of Ag_{14}-F crystals displayed a 1.5-fold enhancement relative to that of Ag_{14}-OMe crystals, which was in sharp contrast to the PL intensity tendency in cluster solutions (Figs. 2B and D). Different from the difference in the PL intensity of cluster solutions that was rationalized from the individual aspect (or the molecular level), the remarkably different PL intensity tendency in cluster crystals should be analyzed from the collective aspect (or the supramolecular level). Therefore, it is safe to propose that the collective effect outweighs the individual effect in the crystal lattice, leading to the opposite trends in emission intensity of the two Ag_{14} nanoclusters in solution or crystalline states. Indeed, the energy dissipation of photo-excited nanoclusters includes two pathways including non-radiative transitions (mainly affected by intramolecular vibrations) and radiative transitions (through PL). From a supramolecular perspective, the fluoride-triggered intercluster interactions would significantly reduce the intramolecular rotations and vibrations of Ag_{14}-F, which would weaken the energy dissipation from non-radiative energy loss [52,53]. Accordantly, the radiative transitions of Ag_{14}-F crystals would be strengthened, resulting in their superior PL intensity relative to Ag_{14}-OMe.

The above-mentioned discussions urged us to further evaluate the intercluster interactions from a supramolecular level of the two Ag_{14} nanoclusters in their crystalline lattices. As depicted in Figs. S10 and S11 (Supporting information), several intracluster interactions were found in both cluster crystal lattices, including $\pi\cdots\pi$, C-H$\cdots\pi$, H$\cdots$H, and H$\cdots$F interactions. However, from the intermolecular aspects, the intercluster interactions of Ag_{14}-F were significantly richer than those in Ag_{14}-OMe. Specifically, the intermolecular interactions in Ag_{14}-OMe were primarily characterized by C-H$\cdots\pi$ and H$\cdots$H interactions (Fig. 3), with C-H$\cdots\pi$ bond lengths ranging from 3.018 Å to 3.802 Å (averagely, 3.41 Å) and H$\cdots$H bond lengths ranging from 2.933 Å to 3.212 Å (averagely, 3.07 Å). In contrast, Ag_{14}-F displayed richer intermolecular interactions, including C-H$\cdots\pi$, C-F$\cdots\pi$, H$\cdots$H, H$\cdots$F, and F$\cdots$F interactions (Fig. 4).

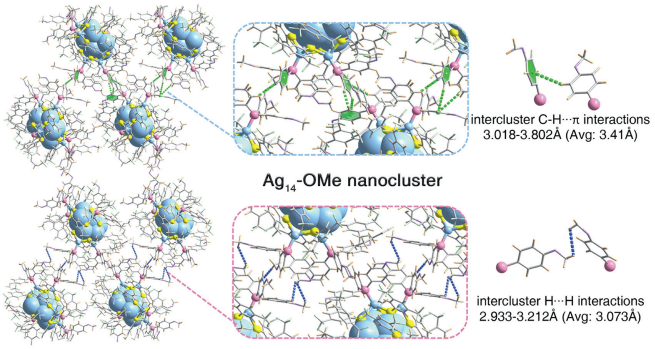


Fig. 3. Schematic diagram of intercluster interactions in the Ag_{14}-OMe nanocluster crystal lattice, including C-H···π (highlighted in green) and H···H (highlighted in blue) interactions.

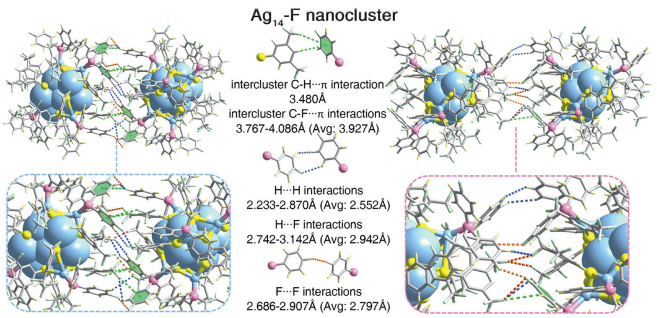


Fig. 4. Schematic diagram of intercluster interactions in the Ag_{14}-F nanocluster crystal lattice, including C-F···π/C-H···π (highlighted in green), H···H/H···F (highlighted in blue), and F···F (highlighted in orange) interactions.

Specifically, the average C-H···π bond length in Ag_{14}-F was 3.480 Å, and H···H bond lengths ranged from 2.233 Å to 2.87 Å (averagely, 2.552 Å). Besides, the C-F···π bond lengths ranged from 3.767 Å to 4.086 Å (averagely, 3.927 Å), and the average H···F and F···F bond lengths were 2.942 and 2.797 Å, respectively. Furthermore, the number of these intercluster interactions in Ag_{14}-F was significantly larger than those in Ag_{14}-OMe (Table S3 in Supporting information). In this context, the abundant intermolecular interactions in Ag_{14}-F gave rise to its more compact packing arrangement in the crystal lattice (Figs. S5 and S6 in Supporting information). Such a more compact packing arrangement of Ag_{14}-F could be further inferred from its lower crystalline packing density relative to that of Ag_{14}-OMe (1.737 *versus* 1.819 g/cm^3). More significantly, although the PL intensity of Ag_{14}-F was much lower than that of Ag_{14}-OMe in the molecular level, the rich intercluster interactions in Ag_{14}-F significantly weakened the intramolecular rotations and vibrations, contributing to a reverse PL intensity tendency, *i.e.*, the superior PL intensity of Ag_{14}-F relative to Ag_{14}-OMe in the crystal lattice.

In summary, based on a structurally comparable Ag_{14} cluster system, we demonstrated that the photoluminescence of metal nanoclusters should be assessed from both the individual and collective aspects. The structure of Ag_{14}-F and Ag_{14}-OMe were essentially identical, with the only difference being the substitution of peripheral phosphine ligands. From the molecular level, the PL intensity of Ag_{14}-OMe was superior to that of Ag_{14}-F due to the stronger electron-donating capability of the P(Ph-OMe)$_3$ ligand, which contributed to a more efficient LMCT process. By comparison, from the supramolecular level, the intermolecular interactions in Ag_{14}-F were significantly stronger than those in Ag_{14}-OMe, limiting the former crystal's non-radiative energy loss and enhancing its PL intensity. Overall, this work presented an interesting cluster pair with comparable molecular/supramolecular structures and interactions, allowing for some new insights into the photoluminescence of cluster-based nano-systems.

Declaration of competing interest

The authors declare no conflict of interest.

CRediT authorship contribution statement

Xiaoqin Du: Investigation. **Peiyao Pan:** Investigation. **Haoqi Li:** Investigation. **Di Zhang:** Investigation. **Wentao Huang:** Investigation. **Xi Kang:** Writing – review & editing, Writing – original draft, Supervision. **Manzhou Zhu:** Supervision.

Acknowledgments

We acknowledge the financial support of the National Natural Science Foundation of China (NSFC, Nos. 22371003, 22101001, and 22471001), the Ministry of Education, Natural Science Foundation of Anhui Province (No. 2408085Y006), the University Synergy Innovation Program of Anhui Province (No. GXXT-2020-053), and the Scientific Research Program of Universities in Anhui Province (No. 2022AH030009).

Supplementary materials

Supplementary material associated with this article can be found, in the online version, at doi:10.1016/j.cclet.2025.111155.

References

[1] R.C. Jin, C.J. Zeng, M. Zhou, et al., Chem. Rev. 116 (2016) 10346–10413.
[2] M.F. Matus, H. Häkkinen, Nat. Rev. Mater. 8 (2023) 372–389.
[3] W.T. Jing, H. Shen, R.X. Qin, et al., Chem. Rev. 123 (2023) 5948–6002.
[4] M. Chi, J. Wei, Z. Zhao, et al., Angew. Chem. Int. Ed. 64 (2025) e202424499.
[5] I. Chakraborty, T. Pradeep, Chem. Rev. 117 (2017) 8208–8271.
[6] R.C. Jin, G. Li, S. Sharma, et al., Chem. Rev. 121 (2021) 567–648.
[7] Y. Du, H. Sheng, D. Astruc, et al., Chem. Rev. 120 (2020) 526–622.
[8] K.Y. Huang, Z.Q. Yang, M.R. Yang, et al., J. Am. Chem. Soc. 146 (2024) 8706–8715.
[9] Y.Q. Feng, F.Y. Fu, L.L. Zeng, et al., Angew. Chem. Int. Ed. 63 (2024) e202317341.
[10] X. Wang, B. Yin, L. Jiang, et al., Science 381 (2023) 784–790.
[11] Y. Horita, S. Hossain, M. Ishimi, et al., J. Am. Chem. Soc. 145 (2023) 23533–23540.
[12] D. Arima, M. Mitsui, J. Am. Chem. Soc. 145 (2023) 6994–7004.
[13] D. Arima, Y. Niihori, M. Mitsui, J. Mater. Chem. C 10 (2022) 4597–4606.
[14] W. Shi, L. Zeng, R. He, et al., Science 383 (2024) 32–33.
[15] S. Masuda, K. Sakamoto, T. Tsukuda, Nanoscale 16 (2024) 4514–4528.
[16] X.J. Zou, X. Kang, M.Z. Zhu, Chem. Soc. Rev. 52 (2023) 5892–5967.
[17] B.D. Peter, W. Pei, G.N. Andrew, et al., Nanoscale 16 (2024) 8090–8095.
[18] T. Chiu, J.H. Liao, Y.Y. Wu, et al., J. Am. Chem. Soc. 145 (2023) 16739–16747.
[19] X.X. Pan, Y.D. Yao, M.X. Zhang, et al., Nanoscale 16 (2024) 8196–8215.
[20] J.T. Zhao, A. Ziarati, A. Rosspeintner, et al., Angew. Chem. Int. Ed. 63 (2024) e202316649.
[21] L.J. Liu, F. Alkan, S.L. Zhuang, et al., Nat. Commun. 14 (2023) 2397.
[22] Z.K. Wang, M.H. Du, P. Braunstein, et al., J. Am. Chem. Soc. 145 (2023) 9982–9987.
[23] J.S. Kim, H. Chang, S. Kang, et al., Nat. Commun. 14 (2023) 3201.
[24] W. Suzuki, R. Takahata, Y. Chiga, S. Kikkawa, et al., J. Am. Chem. Soc. 144 (2022) 12310–12320.
[25] Y.N. Wang, B. Nieto-Ortega, T. Burgi, Nat. Commun. 11 (2020) 4562.
[26] Y.W. Li, M. Zhou, R.C. Jin, Adv. Mater. 33 (2021) 2006591.
[27] X. Wei, K. Chu, J.R. Adsetts, et al., J. Am Chem. Soc. 144 (2022) 20421–20433.
[28] Y. Jin, C. Zhang, X.Y. Dong, et al., Chem. Soc. Rev. 50 (2019) 2297–2319.
[29] W. Ishii, Y. Okayasu, Y. Kobayashi, et al., J. Am. Chem. Soc. 145 (2023) 11236–11244.
[30] Q. Li, C.J. Zeman IV, G.C. Schatz, et al., ACS Nano 15 (2021) 16095–16105.
[31] L. Fang, W. Fan, G. Bian, et al., Angew. Chem. Int. Ed. 62 (2023) e202305604.
[32] Y.X. Chen, M. Zhou, Q. Li, et al., Chem. Sci. 11 (2020) 8176–8183.
[33] K. Kwak, D. Lee, Acc. Chem. Res. 52 (2019) 12–22.
[34] Q. Li, F.Y. Fu, M.Y. Zhao, et al., Chin. Chem. Lett. 36 (2025) 110090.
[35] X. Ouyang, Y.L. Wu, L.J. Guo, et al., Angew. Chem. Int. Ed. 62 (2023) e202300893.
[36] Y.Q. Feng, N.N. Wang, H.X. Ju, Sci. China Chem. 65 (2022) 2417–2436.
[37] D.Y. Wang, X.W. Gao, J.N. Jia, et al., ACS Nano 17 (2023) 355–362.
[38] J. Foxley, K.L. Knappenberger, Annu. Rev. Phys. Chem. 74 (2023) 53–72.
[39] Y. Liu, W. Luo, Q.S. Fan, et al., Adv. Funct. Mater. 33 (2023) 2303470.

[40] O. López-Estrada, B. Zuniga-Gutierrez, E. Selenius, Nat. Commun. 12 (2021) 2477.
[41] Y.W. Li, S. Biswas, T.Y. Luo, et al., Chem. Mater. 32 (2020) 9238–9244.
[42] R.W. Huang, Y.S. Wei, X.Y. Dong, et al., Nat. Chem. 9 (2017) 689–697.
[43] M.M. Zhang, X.Y. Dong, Z.Y. Wang, et al., Angew. Chem. Int. Ed. 59 (2020) 10052–10058.
[44] X. Wei, X. Kang, S. Jin, et al., CCS Chem. 3 (2021) 1929–1939.
[45] S.X. Wang, X.M. Meng, A. Das, et al., Angew. Chem. Int. Ed. 53 (2014) 2376–2380.
[46] X. Kang, S.X. Wang, Y.B. Song, et al., Angew. Chem. Int. Ed. 55 (2016) 3611–3614.
[47] X. Kang, M.Z. Zhu, Chem. Soc. Rev. 48 (2019) 2422–2457.
[48] X. Kang, X. Wei, S.X. Wang, et al., Inorg. Chem. 59 (2020) 8736–8743.
[49] H. Döllefeld, H. Weller, A. Eychmüller, J. Phys. Chem. B 106 (2002) 5604–5608.
[50] J. Zhang, C. Rowland, Y.Z. Liu, et al., J. Am. Chem. Soc. 137 (2015) 742–749.
[51] X. Wei, X. Kang, Z.W. Zuo, et al., Natl. Sci. Rev. 8 (2021) nwaa077.
[52] X. Kang, S.X. Wang, M.Z. Zhu, Chem. Sci. 9 (2018) 3062–3068.
[53] J.S. Xin, J. Xu, C. Zhu, et al., Chem. Sci. 14 (2023) 8474–8482.